

## **Management of Two-Dimensional Channel Flow with a Pair of Streamwise Vortices\*** (Behavior of Streamwise Vortices and Mean Velocity Field)

Shinsuke MOCHIZUKI\*\*, Takatsugu KAMEDA\*\*, Hirotaka YONEDA\*\*\*  
and Hideo OSAKA\*\*

\*\*Graduate School of Science and Engineering, Yamaguchi University,  
2-16-1 Tokiwadai, Ube-shi, Yamaguchi 755-8611, Japan  
E-mail:shinsuke@yamaguchi-u.ac.jp

\*\*\* Mazda Co.Ltd.

3-1 Shinchi, Fuchu-cho, Aki-gun, Hiroshima 730-8670, Japan

### **Abstract**

An experimental study was conducted to examine the management of a two-dimensional turbulent channel flow with a pair of streamwise vortices. A common-flow down type streamwise vortex pair, generated by a pair of half-delta wings mounted on the wall, was introduced into a fully developed turbulent channel flow. The half-delta wings were as high as the inner layer thickness of the channel flow. The mean velocity and Reynolds shear stress distributions were measured and various properties were obtained in order to find meanings of the vortex generator for management of the turbulent channel flow. The convective motion of the secondary current is responsible for most of the streamwise momentum transfer toward the wall in the interaction between the vortices and the shear layer. In the velocity profile averaged over the spanwise extent, the velocity is accelerated below the vortex center and decelerated above the vortex center. Deformation of the mean velocity profile remained at the remarkable downstream distance of 250 times the wing height, which corresponds to 50 times channel the half-width  $H$ .

**Key words:** Turbulent Flow, Flow Control, Secondary Current, Channel Flow, Vortex Generator

### **1. Introduction**

Internal turbulent flows that develop in pipes and ducts are often used in practical engineering applications such as transport lines for fluids or heat transfer in pipes. The effects of wall roughness have been studied for enhancing heat transfer or turbulent mixing in the internal flows<sup>(1,2)</sup>. Recently, experimental investigations have shown that streamwise vortices released from a vortex generator mounted on the wall are effective for enhancing both heat transfer<sup>(3)</sup> and turbulent mixing<sup>(4)</sup>. Mochizuki et al.<sup>(5)</sup> demonstrated that the streamwise vortices generated by three-dimensional roughness on the wall reduce the pressure drop through bends or elbows of transport lines. A possible reduction mechanism was explained under the hypothesis that the secondary current induced by the vortices transports momentum toward the low-pressure side and reduces the pressure difference between the pressure and suction sides. However, no experimental evidence has been

\*Received 25 July, 2007 (No. T1-06-0285)  
Japanese Original : Trans. Jpn. Soc. Mech.  
Eng., Vol.72, No.724, B (2006),  
pp.2955-2961 (Received 20 Mar., 2006)  
[DOI: 10.1299/jfst.2.592]

obtained in the complex three-dimensional turbulent flow field.

Detailed experimental efforts on the momentum transport effect of vortex generators have mostly been performed in turbulent boundary layers<sup>(6-8)</sup>. In the fully developed internal flows bounded by the solid wall, disturbances produce local adverse/favorable pressure gradients or spanwise momentum transport in the cross-streamwise section. In an experimental study on the effect of a pulse disturbance on the fully developed pipe flow, the influence of the disturbance remains over a relatively longer streamwise distance compared with turbulent boundary layers<sup>(9)</sup>. Bradshaw<sup>(10)</sup> reported that disturbances produced by three-dimensional obstacles can be classified into two types: cross-flow vortices and identifiable streamwise vortices. To understand the effect of the secondary current or the extra rate of strain induced by the three-dimensional disturbances, it is necessary to know which types tend to be produced in the internal flows surrounded by the solid wall.

A pair of streamwise vortices is introduced into a fully developed two-dimensional channel flow and distortion and relaxation processes are examined in the mean velocity field. A number of integrated quantities are obtained from experimental data and used to evaluate the momentum transport effect in cross-streamwise planes.

## 2. Nomenclature

$AR$	: aspect ratio ( $=L/(2H)$ ) [ - ]
$c$	: cord length of the half-delta wing [mm]
$H$	: channel half-width [mm]
$h$	: height of half-delta wing [mm]
$L$	: channel width [mm]
$Re$	: Reynolds number ( $=U_c H/\nu$ ) [ - ]
$R_y$	: vortex radius in the y direction [mm]
$R_z$	: vortex radius in the spanwise direction [mm]
$S$	: spanwise separation of the leading edge of the half-delta wings [mm]
$U$	: free-stream velocity [m/s]
$U_c$	: mean velocity at the channel center [m/s]
$U_{ip}$	: approach velocity at the tip of the half-delta wings [m/s]
$V$	: secondary velocity in the y-direction [m/s]
$W$	: secondary velocity in the spanwise direction [m/s]
$x$	: streamwise coordinate [mm]
$x_0$	: streamwise distance measured from the channel inlet [mm]
$y$	: distance from the wall [mm]
$y_g$	: height of the centroid of the mean velocity profile [mm]
$z$	: spanwise coordinate [mm]
$\Omega_x$	: streamwise mean vorticity ( $=\partial W/\partial y - \partial V/\partial z$ ) [1/s]

## 3. Experimental apparatus and techniques

The schematic flow field, as well as the nomenclature and coordinate system used herein, are shown in Fig. 1. The test section of the two-dimensional channel is  $2H = 40$  mm in height,  $S = 700$  mm in width, and 6,000 mm in length. The aspect ratio of  $AR (= S/2H) = 17.5$  is sufficiently large compared to the lower limit value of 7 for the channel flow to be two-dimensional<sup>(11)</sup>. A fully developed two-dimensional turbulent shear flow is established at 80 times the channel height from the entrance with the aide of a tripping device. A pair of half-delta wings mounted on the lower floor of the channel generates a pair of streamwise vortices that is referred to as common-flow up type. The half-delta wing is made of a 0.5-mm-thick bronze plate. The height of the half-delta wing  $h$  is limited to be lower than the inner layer thickness of 4 mm, which corresponds to 143 times the viscous wall length,  $\nu/u_\tau$ . The angle of attack is set to  $15^\circ$ , maintaining the wing plate normal to the wing. The

spanwise separation of the trailing edge of the two wings is adjusted to  $S = 21.5$  mm for the spanwise distance of the two vortex centers to be roughly  $5h$  ( $= 20$  mm). This spanwise width is roughly equal to 700 times the viscous wall length, which is much greater than the spanwise average distance of the streaky structure observed near the wall. The vortex generator is located at  $x_0 = 3,250$  mm ( $= 81.3 \times$  channel height) downstream from the channel entrance, where the flow field reaches the fully developed state.

The Reynolds number based on the maximum center line velocity and channel half width  $H$  was adjusted to 16,000 for all of the experiments. The monotonic static pressure drop is proportional to  $x^{-1}$ , and the standard logarithmic mean velocity profile is confirmed before the pair of streamwise vortices is introduced into the flow. Mean and fluctuating velocity measurements were conducted with constant temperature anemometers and hot-wires probes. A tungsten filament having a diameter of  $2.5 \mu\text{m}$  and an active length of  $0.5$  mm was welded to the tips of the prongs. The active sensor length corresponding to 20 times the viscous wall length has a reasonable spatial resolution for turbulence measurement <sup>(12)</sup>. The instantaneous velocity signals from the anemometers were converted to digital data at the rate of 10 kHz for 10 seconds, and the time averages were calculated using a personal computer system. In the data reduction procedure from the velocity signal to statistical quantities, turbulence terms are neglected in the calculation of mean velocities and secondary current and higher order moments are neglected in the calculation of Reynolds stresses. The uncertainties due to neglecting these additional terms are estimated to be 6.5% for mean velocities and 18.3% for Reynolds shear stresses.

#### 4. Results and discussion

##### 4.1 Behavior of the streamwise vortex pair

The secondary velocity vectors and contour maps of the streamwise vorticity at representative cross-stream sections are given in Figs. 2 and 3. The 'x' symbol indicates the vortex center, which is defined as the location of the maximum streamwise vorticity. These figures show that the common-flow up type streamwise vortex pair is generated by the wings and decays in the downstream direction. The maximum observed secondary vectors are  $0.33U_c$ ,  $0.20U_c$ , and  $0.09U_c$  at  $x/h = 5$ , 10, and 30, respectively. Note that spanwise velocity component  $W$  is greater than the vertical velocity component  $V$  for the maximum values. Outside of the generated streamwise vortex pair, small areas of streamwise vorticity with the opposite sign are recognized near the wall. These small areas are likely induced by the primarily streamwise vortex due to the wall restriction. The spanwise separation of the two streamwise vortices gradually becomes larger, and the vortex center moves away from the wall in the streamwise direction.

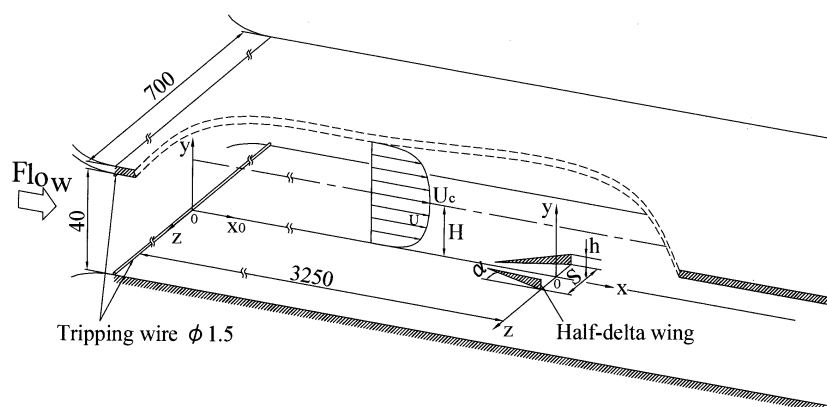


Fig.1: Schematic of flow field, coordinate system, and nomenclature.

The revolution of the maximum streamwise vorticity and the path of vortex center of the streamwise vortex pair are plotted as functions of streamwise travel distance and are compared to the other results in Figs. 4, 5, and 6. The results in the boundary layer<sup>(13)</sup> and the plane turbulent wall jet<sup>(14)</sup> were obtained experimentally using the same common-flow up type of streamwise vortex pair. The symmetry of the revolution process of the vortex pair is shown in Figs. 2 and 3. In the present study, the decay of the maximum streamwise vorticity, as shown in Fig. 4, is that of the positive vorticity observed in the cross-streamwise plane of  $z > 0$ . The definition of vortex radius is the distance from the center to the location at which the streamwise vorticity is equivalent to half the maximum value in the same cross-streamwise plane. Average values calculated from the spanwise and vertical distances are plotted in Fig. 6. The spanwise and vertical positions of the vortex center in Fig. 5 are averages of two streamwise vortices. The least squares method provides approximating curves:

$$[\Omega_x]_{\max} \cdot h / U_{tip} = A \cdot \exp(B \cdot x / h), \quad (1)$$

from each experimental result of decay of the maximum vorticity. Coefficients A and B are numerical constants. Coefficient B, which denotes the degree of decay, is -0.086 for the present channel flow, -0.028 for the boundary layer, and -0.137 for the plane wall jet. In

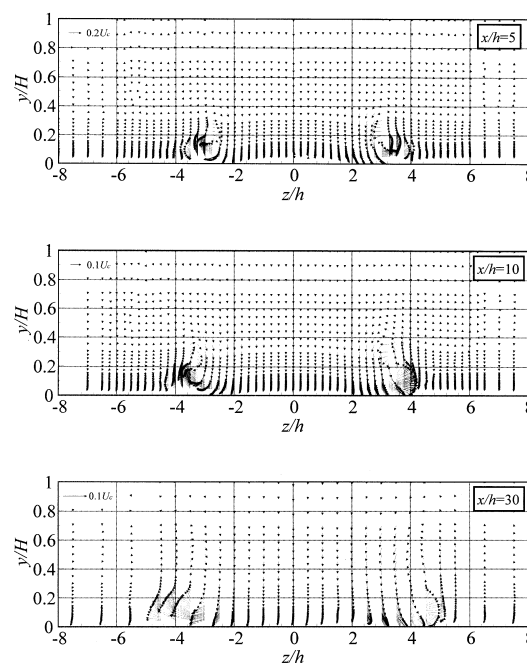


Fig. 2: Velocity vector plot of the secondary current in vorticity in the representative cross-streamwise planes.

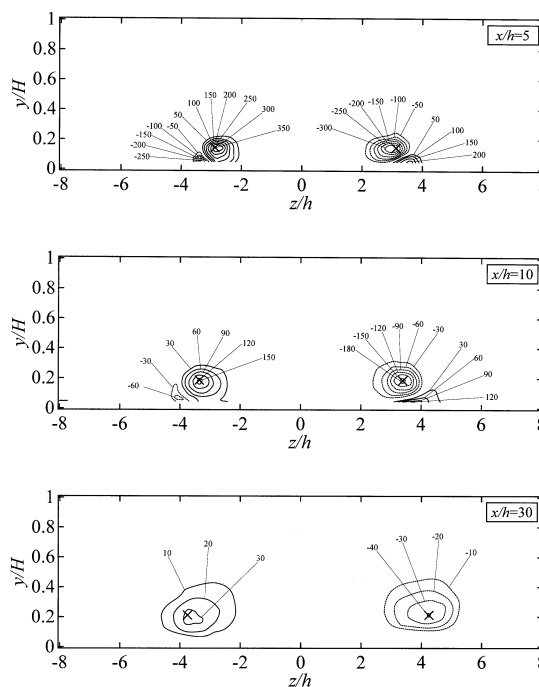


Fig. 3: Contour maps of the streamwise mean vorticity in the representative cross-streamwise planes.

consideration of the condition that the experiments were produced under weak adverse pressure gradients in the boundary layer and a plane wall jet and under a favorable pressure gradient in the present channel flow, the decay rate may not depend only on the pressure gradient. In the boundary layer experiment, the vortex center is located in the outer layer and turbulent intensity around the vortex is a few percent of the free stream velocity. Otherwise, the turbulence intensities around the streamwise vortex are very high, 10% and 20% for the reference velocity in the channel flow and plane wall jet, respectively.

Turbulent diffusion contributes to the increase the vorticity, the growth of the vortex radius, and the decay of the maximum streamwise vorticity. Note that turbulent strength is responsible for revolution of the streamwise vortices. The displacement of the vortex center in the spanwise direction is larger in the boundary layer experiment. Although the strong shear of the mean velocity distribution influences the behavior of the streamwise vortices, the path of the vortex center is determined primarily by the velocity induced by mirror image vortices against the wall. Calculation by the Biot-Savart law can reasonably predict the path of the streamwise vortices. In the boundary layer, the strengths and interactions of the streamwise vortices are maintained for relatively farther downstream. Certain differences of three experiments appear in the revolution of the spanwise radius. In the plane wall jet, the growth of the spanwise radius of the streamwise vortices is much faster than those in the channel flow and the boundary layer. However, in the path and vortex radius of the vertical direction, no

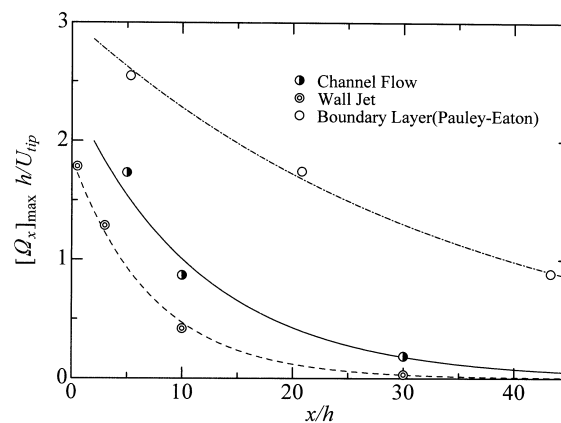


Fig. 4: Decay of maximum value of streamwise mean vorticity and comparison with results in a plane turbulent wall jet and boundary layer.

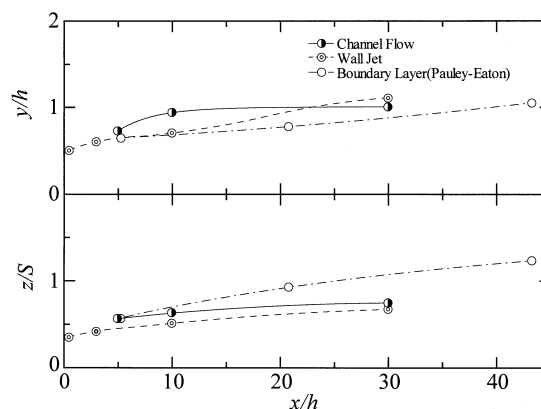


Fig. 5: Path of the streamwise vortex pair.

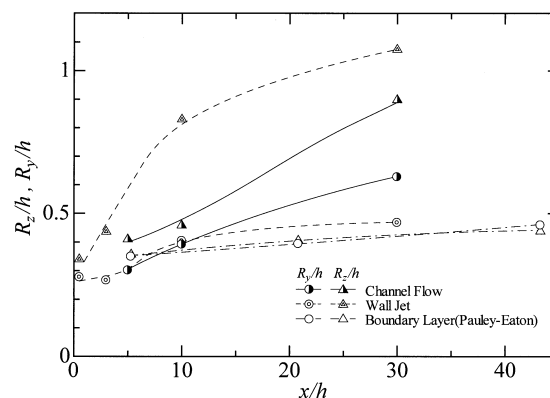


Fig. 6: Development of streamwise vortex radius.

significant difference can be found. The existence of the solid wall likely restricts the growth of the vortex radius normal to the wall.

#### 4.2 Modification of the mean velocity field

Next, we consider the effect of flow management on the mean velocity field modified by the streamwise vortex pair. A contour map of the mean velocity normalized with the centerline velocity  $U_c$  is given in Fig. 7 for the three representative cross-streamwise sections. The vortex center is denoted by the symbol 'x' in each plane. The contour map shows the velocity deficit near the vortex center that is likely due to the local streamwise adverse pressure gradient in the vortex core and the momentum deficit caused by the drag of the vortex generator. The wall-ward secondary current over the spanwise area between the two vortices transports high streamwise momentum near the wall. Otherwise, the upward secondary current induced by the vortices transports low streamwise momentum away from the wall. These momentum transports by the secondary current make the mean velocity gradient near the wall high between the two vortices and low outside the vortices. These high and low mean velocity gradients can be still recognized on the contour map at  $x/h = 30$ .

The mean velocity profile along the centerline is plotted along the transverse direction

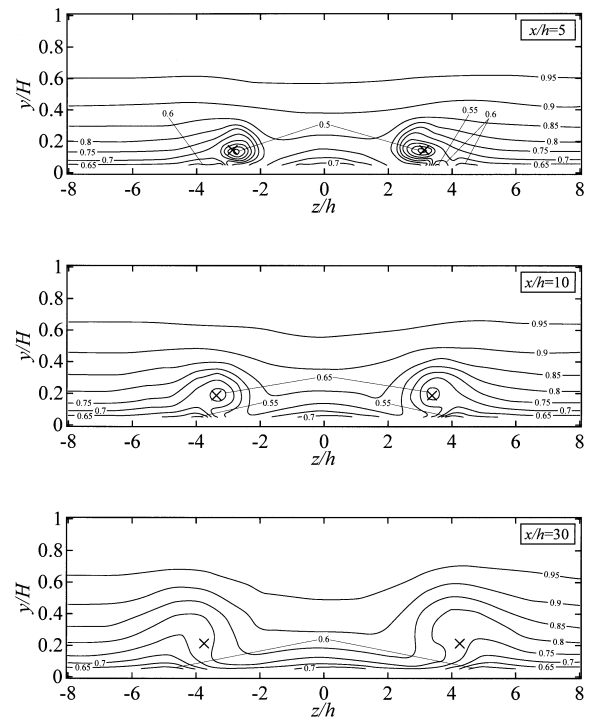


Fig. 7: Contour map of the mean velocity in representative cross-streamwise planes.

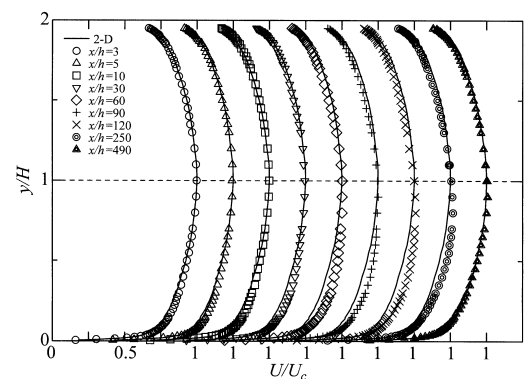


Fig. 8: Mean velocity profile along center line.

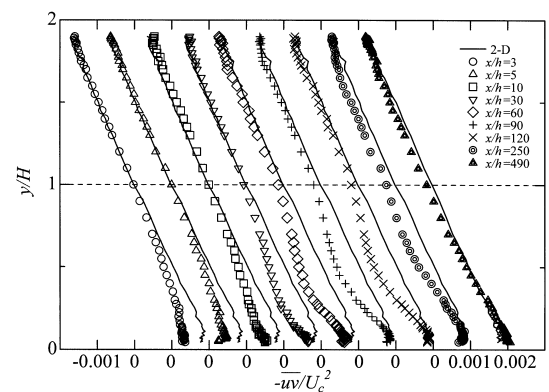


Fig. 9: Reynolds shear stress profiles along center line.

over the entire streamwise distance of  $x_0/h = 3$  to 490. The solid line denotes the mean velocity profile in the non-disturbed two-dimensional flow. The mean velocity near the bottom wall is accelerated due to the momentum transport by secondary current, as shown in Fig. 7. The acceleration can be recognized at a considerably long streamwise distance from the disturbance, at  $x/h = 250$ . A deceleration in the mean velocity profile is found near the upper wall over the streamwise distance of  $x/h = 3$  to 250. This streamwise distance corresponds to 50 times the channel half height. It is seen that the deformation in the mean velocity remains over a considerably long streamwise distance in the channel flow.

The Reynolds shear stress profiles are plotted in the entire layer over the range  $x/h = 3$  to 490 in Fig. 9. The Reynolds shear stress is reduced in the bottom side, where the secondary current is a wall-ward flow. Over the streamwise vortices, the deduction of the Reynolds shear stress is consistent with the smaller derivative of the mean velocity profile flattened by the wall-ward momentum transport. However, the reduction of the Reynolds shear stress near the wall can not be explained by the mean velocity gradient alone, especially at the immediate downstream locations of the disturbance,  $x/h = 3$  to 5. We should at least consider convection from upstream by the mean flow and several rates of strain and should acquire experimental evidence in the complex turbulence field in the vicinity to the vortex generator. In the present study, it is impossible to accurately measure the mean velocity and turbulence quantities using the standard hot-wire technique in such a high-turbulence area.

In order to quantitatively clarify the effect of flow management by the streamwise vortices, the momentum flux due

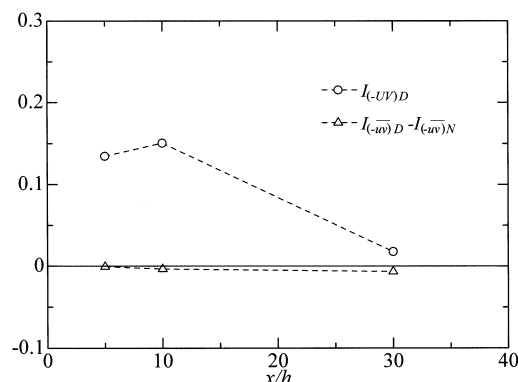


Fig. 10: Streamwise momentum flux integrated in the cross-streamwise planes.

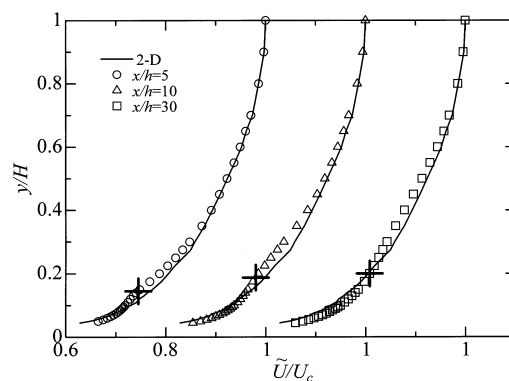


Fig. 11: Mean velocity profile spatially averaged over spanwise direction. The symbol 'x' denotes the vortex center position.

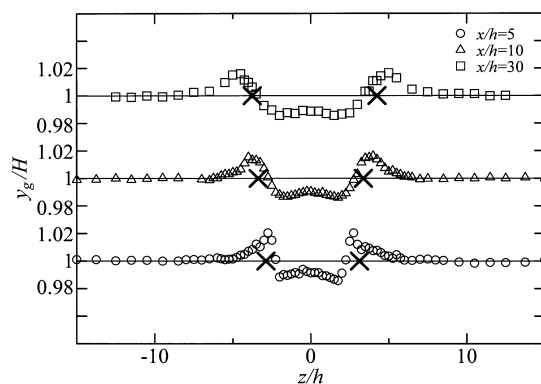


Fig. 12: Spanwise distribution of the centroid of the mean velocity profile. The symbol 'x' denotes the vortex center position.

to the secondary current and the turbulent motions integrated in the cross-streamwise plane are defined as

$$I_{(-UV)} = \left\{ \int_{-z_\infty}^{+z_\infty} \int_0^H (-UV) dy dz \right\} (U_c^2 h H) \quad (2)$$

and

$$I_{(-uv)} = \left\{ \int_{-z_\infty}^{+z_\infty} \int_0^H (-\overline{uv}) dy dz \right\} (U_c^2 h H), \quad (3)$$

where  $z_\infty$  is the spanwise position at which the mean velocities agree within 1% between the non-disturbed flow and the disturbed flow. The integrated values are obtained at the three representative planes and are compared in Fig. 10. The momentum flux due to turbulent motions is subtracted from the flux in the non-disturbed channel flow. Namely, the difference from the two-dimensional flow is plotted in the figure. The secondary current plays a dominant role in the momentum transport by introducing streamwise vortices. The positive value of the integral defined in equation (2) indicates the streamwise momentum flux toward the wall. The turbulent motions contribute little to the enhancement of momentum transport in the entire cross-streamwise plane.

The mean velocity profiles averaged over the spanwise extent for the integrations defined in equations (2) and (3) are shown in Fig. 11. The solid lines and the symbol 'x' denote the mean velocity profile in the two-dimensional flow and the position of the vortex center, respectively. The averaged mean velocity is decelerated over the vortex center and accelerated under the vortex center. The acceleration and deceleration in the averaged mean velocity profile indicates that the introduced vortices transport streamwise momentum toward the wall. Since the fully developed channel flow has no entrainment, i.e., no free-stream flow, transport due to the secondary current causes a redistribution of momentum in cross-streamwise plane. Equation (4) defines the centroid of the mean velocity profile, which is a measure of the redistribution of streamwise momentum:

$$y_g = \frac{\int_0^{2H} U \cdot y dy}{\int_0^{2H} U dy} \quad (4)$$

The centroid  $y_g$  is calculated for the three representative cross-streamwise planes, and the spanwise distributions of the centroid are plotted in Fig. 12. The centroid in the two-dimensional symmetrical flow is located at the channel center  $y_g = H$ . The centroid moves toward the wall in the spanwise direction between the two vortices, and, conversely, moves away from the wall outside the vortex pair. The displacement of the centroid between the two vortices corresponds to 1.5% of channel half-width  $H$  and 7.5% of vortex generator height  $h$ . Note that the streamwise vortex pair successfully maintains the streamwise momentum near the wall and moves the streamwise momentum away from the wall. Since there is no entrainment in the channel flow, fluid moves toward the wall over a certain spanwise distance and fluid moves away from the wall over another spanwise distance for the mass conservation. In outer flows, such as the plane wall jet, acceleration and deceleration of the mean velocity corresponds to the downwash and up-wash of the secondary current<sup>(15)</sup>.

## 5. Conclusions

- (1) The mean velocity is accelerated near the wall in the spanwise direction between the two streamwise vortices. Most of momentum flux due to introducing the streamwise vortex pair is generated by the secondary current.
- (2) The deformation of the mean velocity profile remains for a remarkable distance downstream equal to 250 times the wing height, which corresponds to 50 times the channel half-width  $H$ .
- (3) In the channel flow, transport by the secondary current causes redistribution of the

streamwise momentum flux. The mean velocity profile averaged over the spanwise direction has acceleration near the wall and deceleration away from the wall.

### References

- (1) Dipprey, D.F. and Sabersky, R.H., Heat and Momentum Transfer in Smooth and Rough Tubes at Various Prandtl Numbers, *Int. J. Heat Mass Transfer*, Vol.6, (1963), pp.329-353.
- (2) Kader, B.A. and Yaglom, A.M., Heat and Mass Transfer Laws for Fully Turbulent Wall Flows, *Int. J. Heat Mass Transfer*, Vol.15, (1972), pp.2329-2351.
- (3) Oyakawa, K. and Senaha, I., Heat Transfer Enhancement by Vortex Generators Consisting of Rectangular Blades Insertion in a Duct, *Transactions of JSME, Ser.B*, Vol.65, No.629, (1999), pp.289-295.
- (4) Shioji, M. et al., Evaluation of Mixing Promoted by Triangular Plates in a Channel Flow, *Transactions of JSME, Ser.B*, Vol.67, No.663, (2001), pp.2805-2811.
- (5) Mochizuki, S. et al., Drag Reduction in a 90-degree Bend Pipe with Half-Trip, *Transactions of JSME*, Vol.69, No.679, (2003), pp.595-601.
- (6) Gad-el-Hak, M. and Bushnell, D.M., Separation Control: Review, *Transactions of ASME, J. Fluids Engineering*, Vol.113, (1991), pp.5-30.
- (7) Bushnell, D.M., Longitudinal Vortex Control – Techniques and Applications, *Aeronautical Journal*, (1992), pp.293-312.
- (8) Osaka, H., Flow Control and Management: Drag Reduction Management of Boundary Layer, *Transactions of JSME, Ser.B*, Vol.63, No.605, (1997), pp.2-8.
- (9) Utsunomiya, K., Nishi, S., Nakanishi, S. and Osaka, H., The Measurement of Triple Velocity Correlation behind an Attached Ring-Type Manipulator in Turbulent Pipe, *Transactions of JSME, Ser.B*, Vol.68, No.666, (2002), pp.393-400.
- (10) Bradshaw, P., Turbulent Secondary Flows, *Annual Rev. Fluid Mech.*, Vol.19, (1987), pp.1393-1399.
- (11) Dean, R.B., Reynolds Number Dependence of Skin Friction and Other Bulk Flow Variables in Two-dimensional Rectangular Duct Flow, *Transactions of ASME, J. Fluids Engineering*, Vol.100, (1978), pp.215-223.
- (12) Ligrani, P.M. and Bradshaw, P. Spatial Resolution and Measurement of Turbulence in the Viscous Sublayer Using Subminiature Hot-wire Probes, *Experiments in Fluids*, Vol.5, (1987), pp.407-417.
- (13) Pauley, W.R. and Eaton, J.K., Experimental Study of the Development of Longitudinal Vortex Pairs Embedded in a Turbulent Boundary Layer, *AIAA J.*, Vol.26, No.7, (1988), pp.816-823.
- (14) Mochizuki, S., Nakai, M. and Osaka, H., Structure of a Stronger Wall Jet Managed by a Pair of Streamwise Vortex (Behavior of Streamwise Vortex and Distortion of Mean Velocity Field), *Transactions of JSME, Ser.B*, Vol.66, No.644, (2000), pp.976-984.
- (15) Yamada, S., Experimental Study on the Management of a Stronger Wall Jet, Doctor Thesis of Yamaguchi University, (2004), 73.